ELSEVIER

Contents lists available at ScienceDirect

Mechanics of Materials

journal homepage: www.elsevier.com/locate/mechmat





Determination of elastic and flexural strength properties of multi-scale materials via indentation assisted micro-bending experiment and inverse analysis

Santiago El Awad ^a, Damian Stefaniuk ^{a,b}, Konrad J. Krakowiak ^{a,*}

- ^a Civil and Environmental Engineering Department, Cullen College of Engineering, University of Houston, Engineering Building 1, Room N-132, 4726 Calhoun Road, Houston, TX, 77204-4003, USA
- b Faculty of Civil Engineering, Wroclaw University of Science and Technology, Wybrzeze Wyspianskiego 27, 50-370, Wroclaw, Poland

ARTICLE INFO

Keywords:
Micro-bending
Elastic properties
Mesoscale
Cement composites
Characterization

ABSTRACT

An original approach for mechanical characterization was developed using indentation assisted micro-bending. Aiming at the reliable measurement of elastic modulus of multi-scale solids, the technique relies on deflection measurements of cantilever-type beams modeled within the framework of beams on elastic foundation. The inference of elastic modulus is carried out by postulating the inverse problem and solving it via the error minimization approach. The validation performed on a set of reference materials disclosed the proposed technique's potential for accurate characterization of elastic properties and flexural strength at micro and mesoscale, motivating its extension to heterogeneous materials - cementitious composites in particular.

1. Introduction

With the rapid advancement of testing devices and methods, indentation became a widely popularized and standardized technique for the measurement of mechanical properties of materials on the submicron scale (Doerner and Nix, 1986; Oliver and Pharr, 1992; Oyen and Cook, 2009). The technique pioneered by Brinell and others (Walley, 2012), and the following work by Tabor (1951), allowed for the hardness and yield stress to be linked. On the other hand, classic solutions of contact problem by Hertz (Timoshenko and Goodier, 1970), which were developed for linear elastic solids, paved the way for others (Sneddon, 1965; Doerner and Nix, 1986; Oliver and Pharr, 1992; Oven and Cook, 2003) to assess elastic, plastic, and viscoelastic properties of solids from the load - displacement (P-h) diagram obtained with modern, high-resolution depth-sensing indentation instruments. The versatility of the method has been demonstrated on various material systems spanning across a broad spectrum of constitutive behavior including metals (Oliver and Pharr, 1992; Lucas & Oliver, 1999), ceramics (Oliver and Pharr, 1992; He and Swain, 2007), polymers (Asif and Pethica, 1998; VanLandingham, 2003), or biological tissues (Oyen, 2006).

The classical Hertzian theory (Timoshenko and Goodier, 1970), and its subsequent refinements to inelastic solids (Tabor, 1951; Johnson, 1985), model the indentation problem as a deformation of the half-space

by the elastic punch with non-conforming surfaces, Fig. 1a. Upon contact between the indenter probe and the surface of the material the contact pressure develops over a finite area, the latter is considered to be small compared with the characteristic dimensions of two bodies (L). Consequently, the stress and strain fields, which localize in the vicinity of contact asymptotically diminish moving away from the point of contact into the bulk of the sample (Timoshenko and Goodier, 1970; Johnson, 1985). In the absence of characteristic length-scale (d) that is comparable with the characteristic size of the "indentation-interaction" volume (l), the P-h diagram represents the indentation response of the statistically homogeneous material governed by its representative elastic-plastic properties, elastic modulus, E, and hardness, H, respectively. In the case of heterogeneous solids, the length-scale effects arise and the application of indentation must strictly comply to the scale separation condition (Zaoui, 2002; Constantinides et al., 2006), which is of particular importance for multi-scale testing of complex solids.

While the scale separation condition is commonly fulfilled in nano-scale indentation testing e.g. phase properties in cement-based materials (Constantinides and Ulm, 2004), the experimental assessment of upper-scale mechanical properties e.g. mesoscale effective elastic modulus may be severely limited by the nature, size and morphology of the upper scale heterogeneities, Fig. 1c–d. Moreover, a higher indentation force required to activate significantly larger depths may lead to

E-mail address: kjkrak@uh.edu (K.J. Krakowiak).

^{*} Corresponding author.

local material fracture (Cook and Phaar, 1990; Oyen and Cook, 2009), increasing pile-up phenomena (Fischer-Cripps, 2004), or in case of porous materials the consolidation underneath the probe (Fischer-Cripps, 2004). In turn, significant errors and bias may be introduced in the micro-indentation measurements, thus compromising the inference of the elastic-plastic properties and ultimately directing the experimentalist toward conventional macro-scale ASTM testing on the bulk.

To help address these possible shortcomings, and provide the experimentalist with the reliable auxiliary approach to test for the effective elastic and flexural strength properties of complex solids, at mesoscale, the indentation-assisted micro-bending technique is proposed. It represents the miniaturization of the cantilever flexural test and can be executed with ease in the standard micro-indentation platform, thus bypassing the limitations of high-depth micro-indentation. The proposed method explicitly considers all primary mechanisms of deformation and is framed within the Winkler theory to account for the intrinsic compliance of the specimen-holder system without the need for external calibration of this metric. It must be mentioned, nano- and microscale flexural testing have been popularized in recent years to characterize individual microstructural phases in hydrated cement systems (Němeček et al., 2016) or, micro-volumes of hydrated pastes (Gan et al., 2018, 2020). However, reported studies were constrained by several factors limiting method adaptation for routine testing in the materials characterization labs. These are: a) the use of sophisticated instrumentation for in-situ testing and sample preparation such as focus-ion beam microscopy (FIB-SEM) with integrated indentation platform, or micro-dicing equipment, b) an induced sample damage on the stage of specimen manufacturing and preparation e.g. dehydration in high vacuum or, material interaction with ion beam, c) complete or partial negligence of the system compliance and indentation effect leading to systematic errors in the material properties derived from force-displacement diagrams e.g. elastic modulus, and d) small sampled volumes resulting in sparse measurements and an increased statistical sample size e.g. reported coefficient of variation on Young's modulus and flexural strength up to 22% (Gan et al., 2018, 2020). This work demonstrates that the proposed approach, which is focused on the micro and mesoscale testing of elastic and flexural properties, does not face any of the listed phenomena and could potentially be used complementary to well-established indentation technique in the common experimental set-up.

2. Methodology

2.1. Micro-bending equipment and materials

All micro-bending experiments were carried out with the micro-indentation tester MCT3 (Anton Paar, Austria) and 800 μm spherical indenter, Fig. 2. Micro-indenter was equipped with the 30 N load cell, 6 μN load resolution, depth range up to 1000 μm , and 0.03 nm depth resolution. One of the important features of the used instrument is the active reference system, which allows for automatic subtraction of the displacement due to the compliance of the sample-support, as well as eventual displacement caused by the thermal drift. The environmental effect were minimized with the help of a performance enclosure hosting the MCT3 equipment. All measurements were taken at room temperature 20 \pm 2 °C and RH 65 \pm 5%. Samples were installed in the specially machined holder, made of stainless steel, Fig. 2b-d.

A conventional force-controlled indentation protocol, 30 s loading followed by 30 s unloading, has been applied across the entire spectra of investigated materials. For all tests in which the primary objective was the determination of the elastic modulus, the maximum force was selected such that the resultant bending displacement was reversible, and the only residual displacement was due to the indentation effect. Moreover, to reduce the impact of potential non-linear effects e.g. fracture, the maximum tensile stress in the most strained beam's cross-section must not exceed 10% of its flexural strength. In tests focused on the micro-bending flexural strength, selected samples were loaded at a rate of 1 N/min until reaching the critical force, P_{cr} , at rupture. The

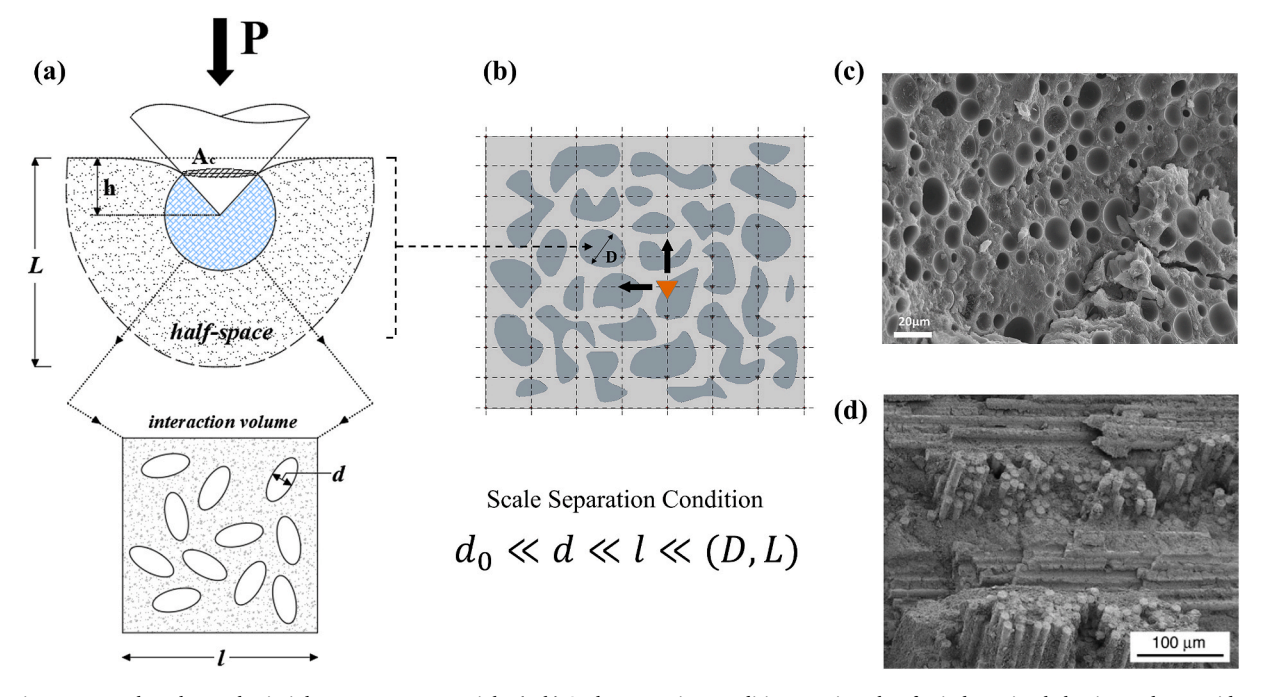
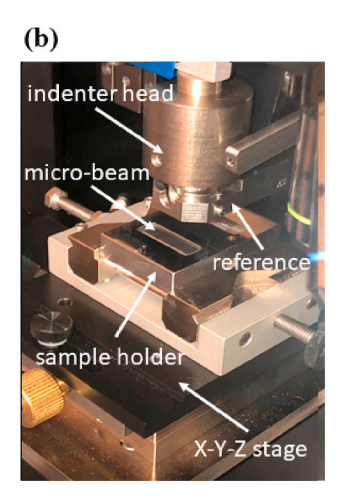
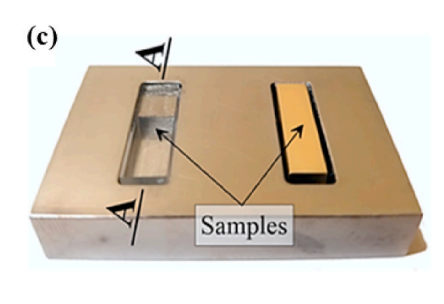


Fig. 1. Microstructure length – scales in inhomogeneous materials. (a–b) Scale separation condition requires that for indentation behavior under consideration the characteristic size of the interaction volume, *l*, to be much larger than the characteristic length of inhomogeneities and deformation mechanism, *d*. Additionally, *l* must be much smaller than the characteristic scale of upper-level inhomogeneities, *D*, and/or the characteristic dimension of the whole body, *L* (Constantinides et al., 2006). (c–d) Examples of ceramic composites for which heterogeneity scale and texture severely limit the application of conventional indentation methods to assess micro, meso-scale effective elastic modulus (c – cement-based composite with hollow glass microspheres, d – mullite-based porous matrix continuous-fiber ceramic composite adopted from Zok (Zok, 2006).







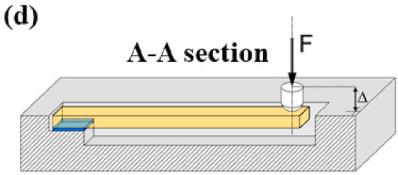


Fig. 2. Indentation assisted micro-bending testing: (a) general view on the micro-indentation testing platform, (b) detailed view on the micro-bending setup installed in the indentation platform, (c–d) perspective and cross-sectional views on the machined sample holder with installed samples of referenced materials.

Modulus of Rupture (MOR) is calculated according to Eq. (1), where w and t are the width and thickness of the specimen, and L is the distance measured from the load application point to the location of fracture on the beam.

$$MOR = \frac{6P_{cr}L}{wt^2}$$
 Eq. 1

Lastly, to assure the accurate force positioning along the longitudinal axis of the beam, and to minimize torsional effects, an optical microscope and motorized XYZ table of micro-indenter were used. Samples were installed into the sample holder using cyanoacrylate adhesive (Super Glue, Loctite).

Materials selected for this study include reference metals and ceramics: stainless steel SS304, aluminum 6061-T65, naval brass, copper, and homogeneous fused silica glass, Fig. 3. Additionally, to test the applicability of the method to heterogeneous solids a mature normal, and lightweight hydrated cement pastes was examined, Fig. 3. The later type of cement composite, which incorporates glass cenospheres, offers an attractive pathway toward achieving high strength low thermal conductivity construction materials that could be used in the engineering of energy-efficient and resilient building envelopes. For example, hollow glass microspheres offer a closed pore structure that reduces the water ingress thus making the cement-composite less vulnerable to moisture changes, due to their low density they effectively contribute to lowering the thermal conductivity of the composite, and their glass shell strengthens the pore walls helping it to sustain local stresses (Krakowiak et al., 2020). However, due to the substantial size variability and the characteristic texture of hollow glass microspheres, microscale testing of lightweight cement composites with classical indentation presents a significant challenge and is commonly restricted to a standard

macroscale characterization. Representative samples of each material were machined to the specified size, $20.00 \times 2.50 \times 5.25$ mm. The sample surface exposed directly to the indenter probe was ground and polished to minimize the effects of surface roughness on the displacement measurements and contact point detection (Miller et al., 2008). Cement paste samples were tested in the saturated surface dry state (Mindes et al., 2002).

3. Micro-bending method formulation

The general idea of the indentation assisted micro-bending method is very much similar to the standard ASTM (ASTM C293, 2016; ASTM C78, 2018) testing methods used in the structural scale testing of constructional materials under flexure. However, given constraints of test miniaturization, as well as the requirement of implementation ease, the cantilever beam scheme has been adapted instead of third-point bending, or center-point bending configuration, Fig. 4. One of the significant advantages of the cantilever approach lays in the considerably higher magnitude of the peak displacement, Δ_B , as compared to simply supported beam under the center load of the same magnitude, which is 1/16 of the former (Timoshenko and Goodier, 1970). Therefore, smaller forces are required to provoke measurable deflection which will be substantially greater than potential displacement due to contact with the rigid probe (indentation displacement), or random displacement fluctuation caused by the environmental effects or material heterogeneities. Moreover, force reduction is also an advantage to minimize the effects of local stress concentration which would activate non-linear phenomena, e.g., plasticity, fracture, thereby, the linear-elastic behavior dominates. Under such conditions, the potential inference of the elastic modulus may be carried out with high accuracy and consistency in the small

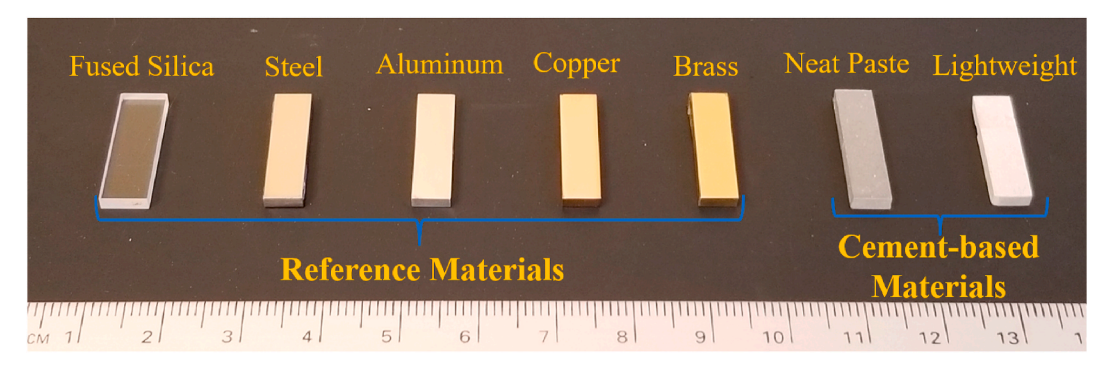


Fig. 3. Overview of materials selected for this study: reference materials and Class G cement-based materials (neat paste and lightweight).

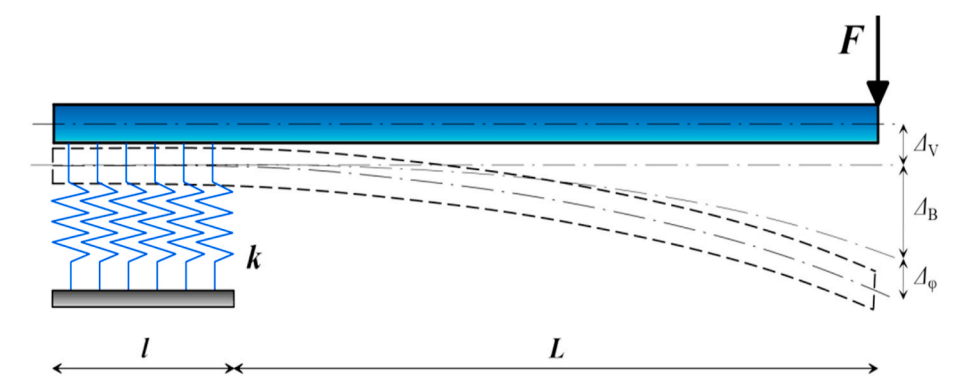


Fig. 4. Mechanical model of the micro-bending experiment. Nonrigid cantilever support gives rise to rotational and vertical compliance effects.

deformation limit.

One of the significant disadvantages of the proposed static scheme is the obvious difficulty in the experimental realization of the "perfectly" rigid support, in which the translational displacements and cross-section angle of rotation are zero. The mechanical clamping of a sample is possible to some extent, however, still it does suffer from a certain level of compliance that would need to be accounted for when analyzing the experimental outcome. Likewise, the use of an adhesive such as cyanoacrylate, which is the most commonly applied method of sample stabilization in small-scale mechanical testing, e.g., instrumented indentation, is also prone to this effect. Therefore, irrespective of the selected method of cantilever support realization in the experimental setup, one should be able to quantify the effects of existing support compliance and discount it from the measured total displacement when estimating elastic stiffness. In the proposed approach, the effect of the elastic support is explicitly considered using the theory of Winkler (Hetényi, 1971), the support of the beam is considered as series of non-interacting linear-elastic springs distributed along the support length, l, whose the collective behavior is described using single stiffness parameter k.

3.1. Mechanical model

The governing relationships of the indentation assisted microbending test are derived considering the static scheme of the cantilever beam on the elastic support, Fig. 4. Accordingly, the application of the point load at the distance L from the support results in the total deflection, $\Delta_{\rm T}$, which is a composite function of: $\Delta_{\rm B}$ - the pure bending displacement, $\Delta_{\rm Q}$, $\Delta_{\rm V}$ – displacements due to rotational and translational compliance of the elastic support, $\Delta_{\rm S}$ – displacement due to shear effect, and $\Delta_{\rm I}$ – indentation displacement, Eq. (2).

$$\Delta_{\rm T} = \Delta_{\rm B} + \Delta_{\rm o} + \Delta_{\rm V} + \Delta_{\rm S} + \Delta_{\rm I}$$
 Eq. 2

The first three components are derived considering the mechanical system presented in Fig. 4 for which the beam deflection must satisfy the fourth-degree differential equation Eq. (3) in the elastic support domain 0, l, and the Euler-Bernoulli moment-curvature equation elsewhere Eq. (4).

$$EI\frac{\partial^4 w}{\partial x^4} + kw = 0 Eq. 3$$

$$EI\frac{\partial^2 w}{\partial x^2} = -M_{\alpha}$$
 Eq. 4

By considering the proper boundary condition on the elastic support part, as well as continuity of the deflection and cross-section rotation, see Appendix I, the sum of the first three components is explicitly given as:

$$\Delta = \underbrace{\frac{\text{FL}^3}{3\text{EI}}}_{\Delta_{\phi}} + \underbrace{L(\theta_{1,F} + \theta_{1,M})}_{\Delta_{\phi}} + \underbrace{(w_{1,F} + w_{1,M})}_{\Delta_{V}}$$
 Eq. 5

where $\theta_{1,F}$, $\theta_{1,M}$, $w_{1,F}$ and $w_{1,M}$ are the cross-section rotations and deflections at the junction of the elastic support and cantilever domain due to the concentrated force F and bending moment M = FL, respectively. Detailed step-by-step derivation of Eq. (5), as well as explicit definitions of involved quantities, are presented in Appendix I.

3.1.1. Shear correction

The Euler-Bernoulli beam theory applies to slender beams in which the length dominates cross-sectional dimensions (Timoshenko and Goodier, 1970). Usually, as a rule of thumb, the span of the beam should be much greater than its height, $L\gg h$, so the effect of shear stress on the beam deflection can be neglected. However, the preparation of slender beams for the proposed micro-bending method may present certain difficulties related to sample processing, e.g., cutting, grinding. Such difficulties very often arise when working with brittle materials, e.g., cement paste, glass, in which locally exerted stress on the sample during the preparation stage can lead to fracture. Therefore, from the practical point of view beams of slightly greater flexural stiffness are more convenient to work with. Given this, it may be necessary to account for the shear deformation effect and employ the necessary correction. According to Timoshenko beam theory (Timoshenko and Goodier, 1970), which takes into account the effect of shear deformation on the beam deflection, for cantilever this extra displacement is given as:

$$\Delta_s = \frac{FLh^2}{8GI},$$
 Eq. 6

where G is the shear modulus of the beam material, in which the Poisson ratio (ν) of 0.25 is considered. It must be noted, given that the shear effect is diminishing for longer spans, it is one of the smallest contributors to the total measured deflection, and for most construction materials of interest ν varies from 0.1 to 0.4. Such an assumption has a negligible effect on the estimated elastic modulus, however, if more accurate estimate of ν is available, its substitution into the inverse problem is recommended e.g. 0.17 for fused silica.

3.1.2. Indentation displacement component

By the design, the static scheme of the micro-bending experiment assumes the point load is delivered to the beam. However, such an idealized condition cannot be realized in practice, and the load is transferred with the help of a rigid indenter (see Fig. 1a). As such, the concentrated force is distributed over the contact area, thus, provoking local deformation and displacement fields. Therefore, the total displacement at the point of load application measured in the microbending experiment has a built-in displacement corresponding to the indentation, $\Delta_{\rm I}$, which needs to be accounted for. The amount of

indentation displacement can be modified by changing the geometry of the indenter probe. For example, the Berkovich and Vickers tips are the most commonly used probes in standard indentation (Fischer-Cripps, 2004). Due to their pyramidal shape both lead to strain localization and the development of a plastic zone, which for medium and large indentation forces result in fracture in brittle materials (Cook and Phaar, 1990). One way to minimize stress concentration effects and plastic zone development is to reduce the average pressure under the indenter and select the indenter of axisymmetric geometry, e.g., spherical. The effect of plastic deformations can be mitigated with a spherical indenter, although not necessarily eliminated, this depends on the depth-to-radius ratio as well as the elastic-plastic properties of the indented material. Therefore, the displacement due to indentation, $\Delta_{\rm I}$, will be treated as an unknown parameter in the inverse problem formulation with a constrain that it should be larger or equal to the one corresponding to the completely elastic deformation described by Hertz's contact theory (Timoshenko and Goodier, 1970).

3.2. Inverse problem formulation

Given the mechanical model formulated previously, the inverse problem is constructed aiming at the estimation of elastic modulus, E. support stiffness parameter, k, and the indentation displacement Δ_I at maximum load F. In this regard, the micro-bending experiment is carried out at multiple spans and according to the same loading protocol, Fig. 5. The estimation of the listed parameters, enclosed in the model vector $\beta = [E, k, \Delta_I]$ is carried out by solving the inverse problem using the leastsquare approach (Chavent, 2010). The objective function that is to be minimized considers the difference (residual) between the experimental observations Δ_i (total displacement measured at a distance L_i from the support) and the model prediction, Eq. (5). To enhance stability to the inverse problem solution and increase the accuracy of the estimated parameters, the objective function includes also the residual term corresponding to the indentation in the center of the elastic support portion of the beam. The analytical solution for the finite-length Winkler type beam deflection under the center point load is described in Appendix II, (Hetényi, 1971). In this work, Matlab® programming environment has been used in the estimation of the parameters.

4. Results and discussion

The detailed experimental results of the micro-bending on selected reference materials are presented next. Three samples were evaluated for each reference solid and Young's modulus was estimated together with the two other model parameters, the stiffness of the support (k) and indentation displacement (Δ_I), respectively. Obtained results from the micro-bending technique are then cross-checked with the literature data

and macroscale properties obtained according to ASTM standard uniaxial testing. Finally, the case of normal weight hydrated cement paste, as well as a more complex microstructure lightweight cement system with hollow glass microspheres are discussed.

4.1. Validation on reference materials

Fused silica force-displacement diagrams are presented in Fig. 6a. As can be observed, the linearity of the F vs. Δ response is amplified with the increasing distance of the force from the beam support. The optimum model fit, Fig. 6b, closely follows the experimental observations across all the considered spans. Thus, the Winkler-Type approximation proposed in this work holds well in explaining micro-bending measurements. Moreover, it demonstrates clearly (as predicted) the mechanical response of the system is increasingly dominated by the bending displacement and support rotational effects, Fig. 6c. Accordingly, as the span length increases bending contribution increases ($\Delta_{\rm B} \propto L^3$) at the greatest rate compared to the other displacement contributors. As for the rotation at the elastic support, here the displacement growth is consistent with the increasing span, however, at a substantially smaller rate $(\Delta_{\phi} \propto L^2)$. The indentation contribution on the contrary is constant along all the spans. However, with increasing span length its percentage contribution becomes less significant compared to other displacements (especially bending and rotational displacements). Shear displacement and the vertical compliance component are the smallest contributors. The observed trends are confirmed for stainless steel, Fig. 6d-f, and hold for other reference materials too.

The estimated values of Young's modulus for all reference materials are reported in Table 1. For all materials, micro-bending based estimates show very good agreement with the values measured in the standard ASTM macroscale testing that are reported in the open literature (ASM, 1990; Oliver and Pharr, 1992; EuroInox, 2007; Callister Jr., 2007; Engineering Edge, 2020), Fig. 7. On the other hand, quite a significant spread is observed in the estimated values of the elastic support stiffness. Despite the entire effort and precautions taken on the sample mounting stage, this result underscores difficulties in controlling the adhesive layer thickness, as well as distribution underneath the sample. Moreover, because only the top surface of the sample directly exposed to the interaction with the indenter has been finely polished, the observed spread must also reflect the overall variability of the interfacial bond due to the contact surface of various levels of roughness. However, as can be noticed, this effect has no impact on Young's modulus estimate, which is the primary metric assessed in the micro-bending test proposed in this work. Presented results on reference materials validate the proposed micro-bending method as an efficient means of inference of elastic modulus at micro and mesoscale.

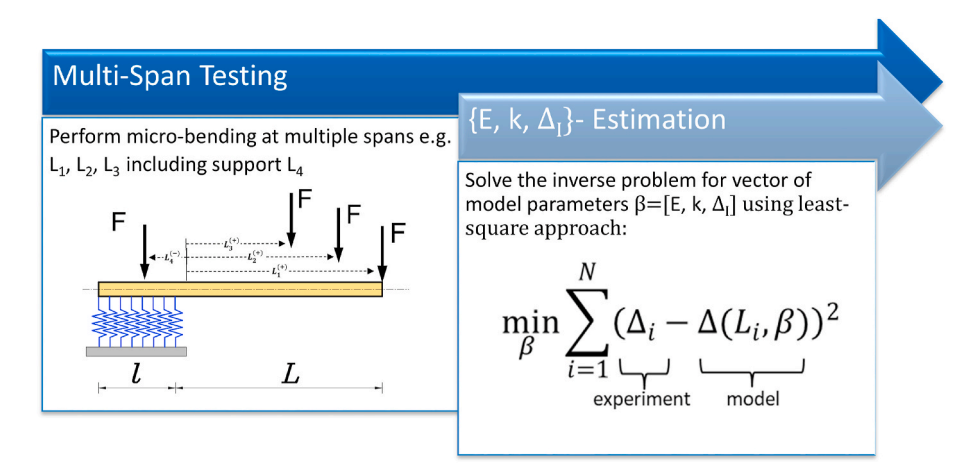


Fig. 5. Implementation of the inverse problem by utilization of multiple spans micro-bending testing.

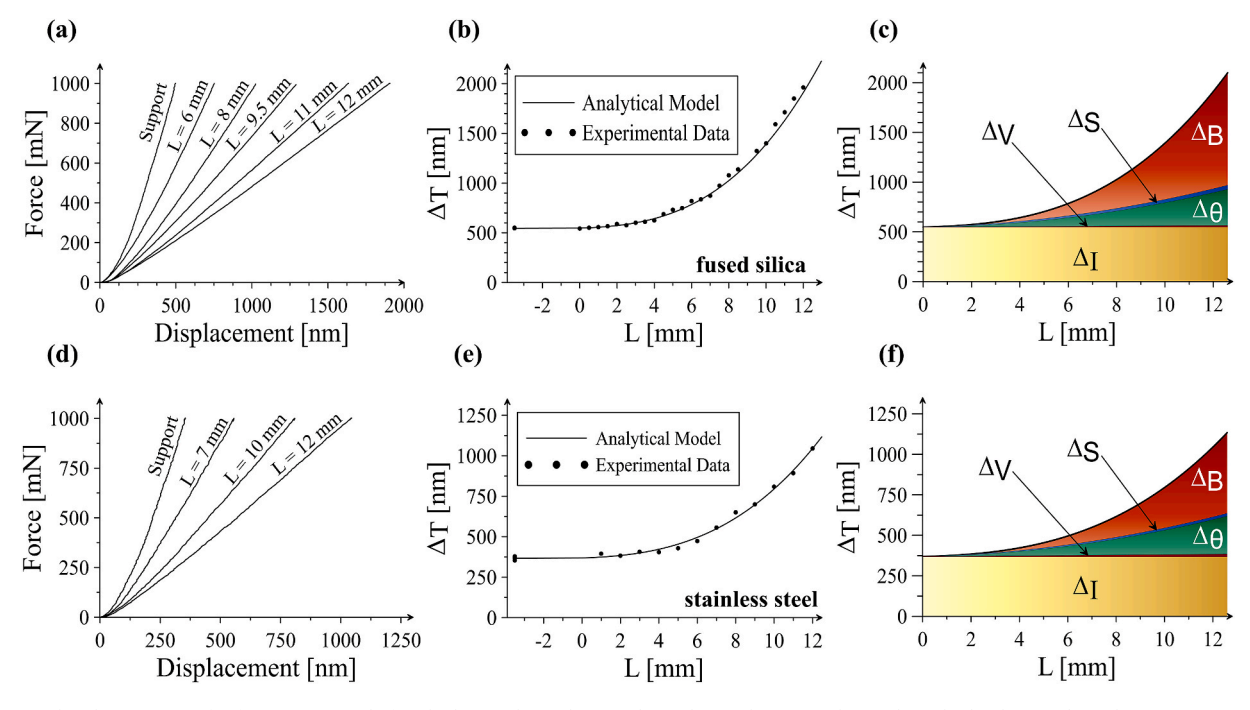


Fig. 6. Micro-bending testing of reference materials fused silica and stainless steel: (a, d) P- Δ diagrams obtained on the loading cycle and at various spans, (d, e) optimum fit of the analytical model to the experimental data, and (c, f) the contribution of various components of the total measured displacement.

Table 1 Estimates of Young's modulus (E), the stiffness of the support (k), and indentation displacement Δ_{I} , obtained in the inverse analysis on reference solids.

Material	E [GPa]	k [GPa]	$\Delta_{\rm I}$ [nm]	Error [%] ^a
Fused silica	70.2	870	546	< 1 (< 3)
	73.3	520	565	
	72.1	1090	520	
SS304 Steel	201.9	930	379	< 2 (< 5)
	201.4	470	366	
	189.4	870	794**	
Aluminum	68.4	1075	690	< 1 (< 2)
	68.7	610	661	
	69.8	980	1293**	
Copper	119.3	1200	366	< 3 (< 5)
	114.1	951	383	
	127.4	1200	611**	
Brass	107.5	448	511	< 6 (< 8)
	105.1	484	508	
	103.7	634	458	

a relative error with respect to the literature reported data, for an average of group error and in parenthesis largest individual error: fused silica 72 GPa (Oliver and Pharr, 1992), stainless steel 200 GPa (EuroInox, 2007), aluminum 69 GPa (Callister Jr., 2007), copper 117 GPa (Engineering Edge, 2020), and naval brass 100 GPa according to ASM International Handbook (ASM, 1990), ** - 200 μm spherical indenter probe used.

4.2. Application to cementitious systems

Given the theoretical framework and experimental verification of the reference materials presented in the previous paragraph, the microbending technique is now applied to a more complex class of materials, cementitious solids. The experimental results on normal weight Class G cement paste and lightweight cement Type II paste are presented in Figs. 8 and 9 and Table 2. A more detailed description of the lightweight cement paste microstructure with hollow glass microspheres may be found elsewhere (Krakowiak et al., 2020).

The values of Young's modulus obtained through the micro-bending technique for the cement paste samples are reported in Table 2. The average E value obtained from three investigated samples of Class G

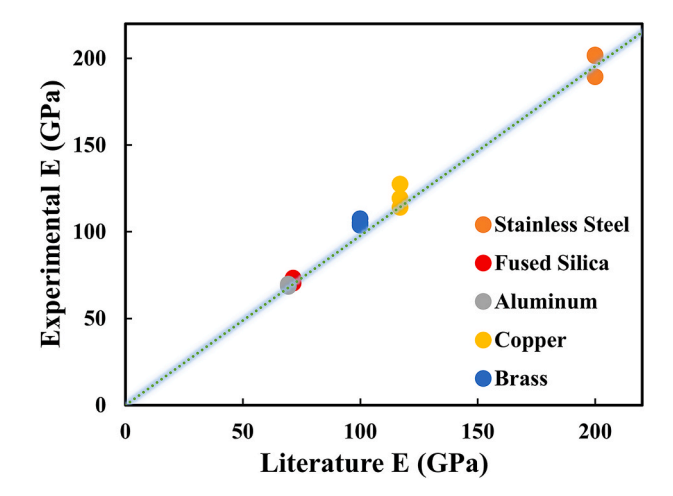


Fig. 7. Comparison of the micro-bending estimates of Young's modulus (*E*) with the macroscopic values assessed in standard ASTM testing and reported in the open literature (ASM, 1990; Oliver and Pharr, 1992; EuroInox, 2007; Callister Jr., 2007; Engineering Edge, 2020).

cement paste is 17.4 GPa with a standard deviation of 0.6 GPa, which accounts for a coefficient of variation of 3.4%. On the other hand and as expected, the average elastic modulus of the lightweight Type II cement system is significantly lower, 10.3 GPa with a coefficient of variation of 4.8%. Given the triplet of E, k and Δ_I parameters that correspond to the best fit, the individual contributions of displacements could be decoupled, and similar trends to the one previously described for reference materials hold, Fig. 8a–c. In both cases, micro-bending estimates show very good agreement with the elastic modulus measured in the standard ASTM macroscopic tests, Table 2. The relative error on the former is less than 5% and less than 4% in the latter case. This strongly suggests that despite two orders of magnitude difference in the probed material volume the micro-bending estimates captures statistically homogenous material response similar to macro-scale testing of the bulk pastes.

The versatility of the micro-bending technique is vast. Besides

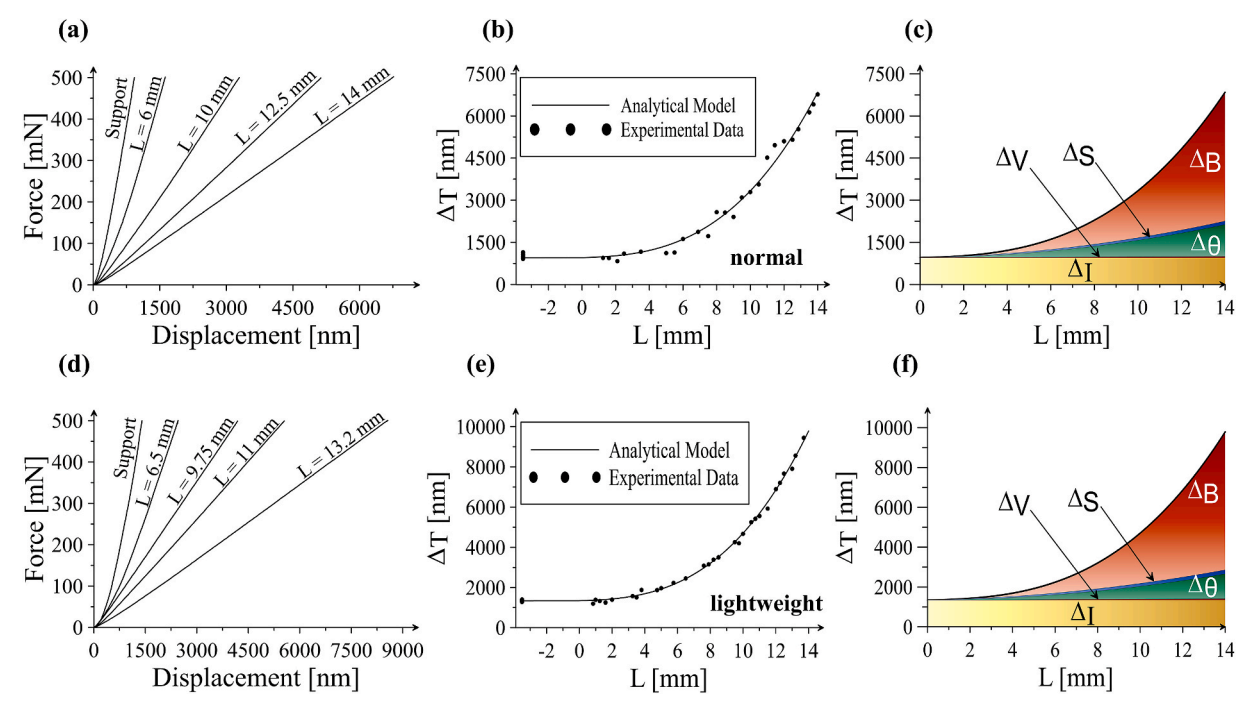


Fig. 8. Micro-bending testing of neat and lightweight cement systems: (a, d) *P-Δ* diagrams obtained on the loading cycle and at various spans, (d, e) optimum fit of the analytical model to the experimental data, and (c, f) the contribution of various components of the total measured displacement. Neat cement paste tested at the age of 8 months.

Table 2 Estimates of Young's modulus (E), the stiffness of the support (k), the indentation displacement Δ_1 , and flexural strength of cement-based composites.

Material	E [GPa]	k [GPa]	$\Delta_{\rm I}$ [nm]	MOR [MPa] ^a	Error [%]**
Neat Paste	17.6	206	915	13.6 ± 2.0	< 5
	16.7	129	845		
	17.8	102	939		
Lightweight	10.2	955	1293	9.5 ± 1.9	< 4
	9.9	600	1340		
	10.8	125	1170		

^a modulus of rupture (MOR) average value and standard deviation estimated from 28 samples for Class G paste, and 3 for the lightweight Type II cement paste.

providing the access to elastic modulus, the non-linear mechanical characteristics of the investigated cementitious solid can be explored for the specimen of interest, e.g., modulus of rupture, Table 2. This gives the researcher straight forward access to two quantitative metrics of mechanical performance of the material in question extracted from sequential testing of the same specimen akin to the pair of elastic modulus and hardness assessed in the classical indentation testing (Oliver and Pharr, 1992). Moreover, the small size of the specimen together with simple geometrical form, and easy to execute preparation protocol, allow executing testing campaigns with an increased number of samples, thus improving the confidence intervals of the estimated properties without significantly expanding on testing time. This is of particular importance when a bulk solid is available in a very limited amount such that macro-scale tests are not feasible, or multi-scale parametric study of processing-microstructure-performance link is carried out prior to structural scale testing of the most promising material system. Additionally, the test miniaturization proposed here offers a unique opportunity in performing microstructural investigation of damage development and localization (using electron microscopy, SEM) before and after mechanical testing in indentation-assisted

micro-bending, see Fig. 9. However, one needs to be aware of the size effect (Bazant and Novak, 2001; Novak et al., 2002) and existing differences in the shear force distribution when comparing to center-point of third-point flexural strength.

4.3. Material heterogeneity and surface roughness effects

One of the most critical points in the micro-bending testing, and consequently the analysis of the experimental outcome, is the observed variance on the measured total displacement, Δ_T . In solving the inverse problem (Fig. 5), which employs the least-square approach, higher variance on the measured displacement translates automatically to an increased residual. As a result, the uncertainties on the model parameters $\{E, k, \Delta_I\}$ also increase. While various factors may impact the displacement measurements, the experimental analysis strongly suggests the material heterogeneity and surface roughness dominate. This is in analogy to the instrumented-indentation testing, in which both phenomena are recognized to negatively impact the consistency and accuracy of the force-displacement curve. To illustrate this effect we revisit the analysis results, obtained on reference fused silica and the cement paste, and plot the distribution of residuals $\varepsilon = \Delta_{\text{exp}} - \Delta_{\text{model}}$, Fig. 10.

For fused silica, a homogeneous solid that was prepared at the high surface finish (low surface roughness), the average of 1st and 3rd quartiles is around 10 nm (see Fig. 10). Additionally, the maximum recorded difference between the median residual and its min. and max. value is around 30 nm. Such narrow distribution of residuals suggests consistent displacement measurements. This is in significant contrast to neat cement paste, for which the distribution of residuals is much broader (Fig. 10), and the extreme values can differ by up to 250 nm from the median depending on the location of the indenter probe. It is known, cement paste is highly heterogeneous. Therefore, at certain locations, the indenter may activate the interaction volume which incorporates heterogeneities such as clusters of residual belite, or large capillary pore. In such situations, the fulfillment of the scale separability condition may be weak and the micro-bending response will show discrepancy as compared to the average trend. This discrepancy will be

^{**} relative error with respect to the standard macroscopic ASTM testing: neat paste 18.2 \pm 0.6 GPa and lightweight 10.7 \pm 0.6 GPa.

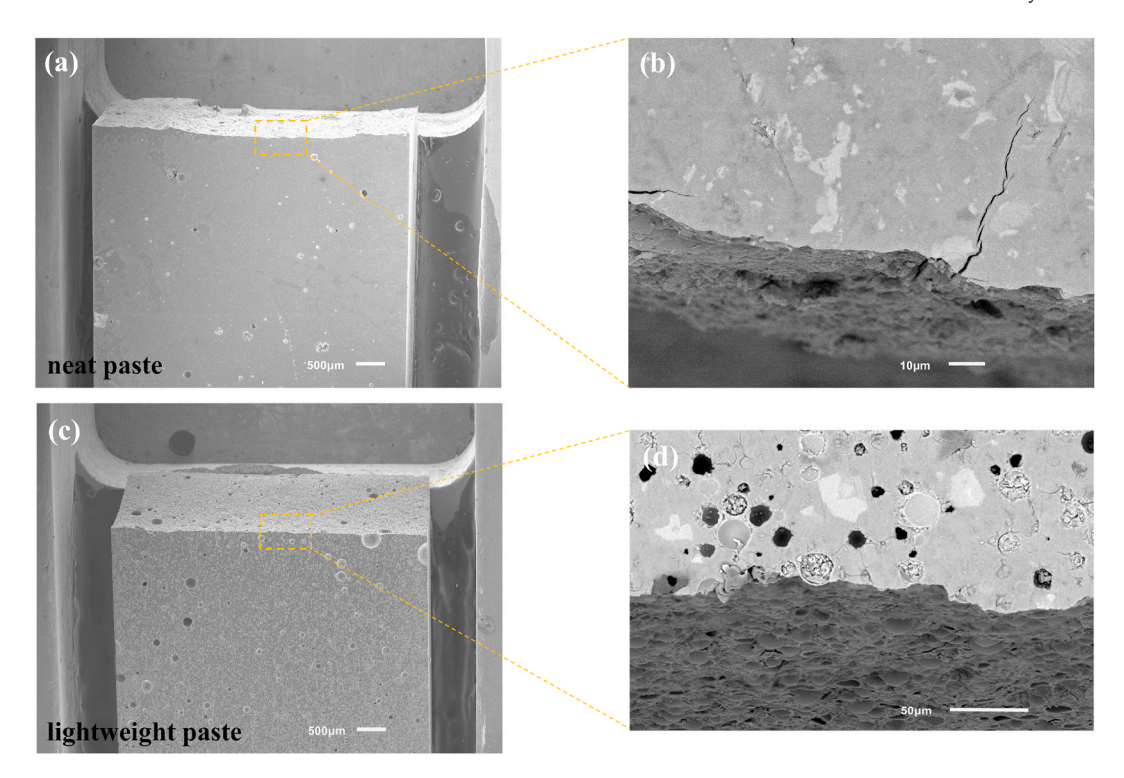


Fig. 9. Secondary electron (SE) micrographs of fractured beams of neat (a) and lightweight cement paste with hollow glass high strength microspheres (b) installed in the stainless steel holder and after flexural strength tests using developed micro-bending approach. Detailed SEM-BSE image of the portion of the fractured surface in neat (b) and lightweight cement paste (d).

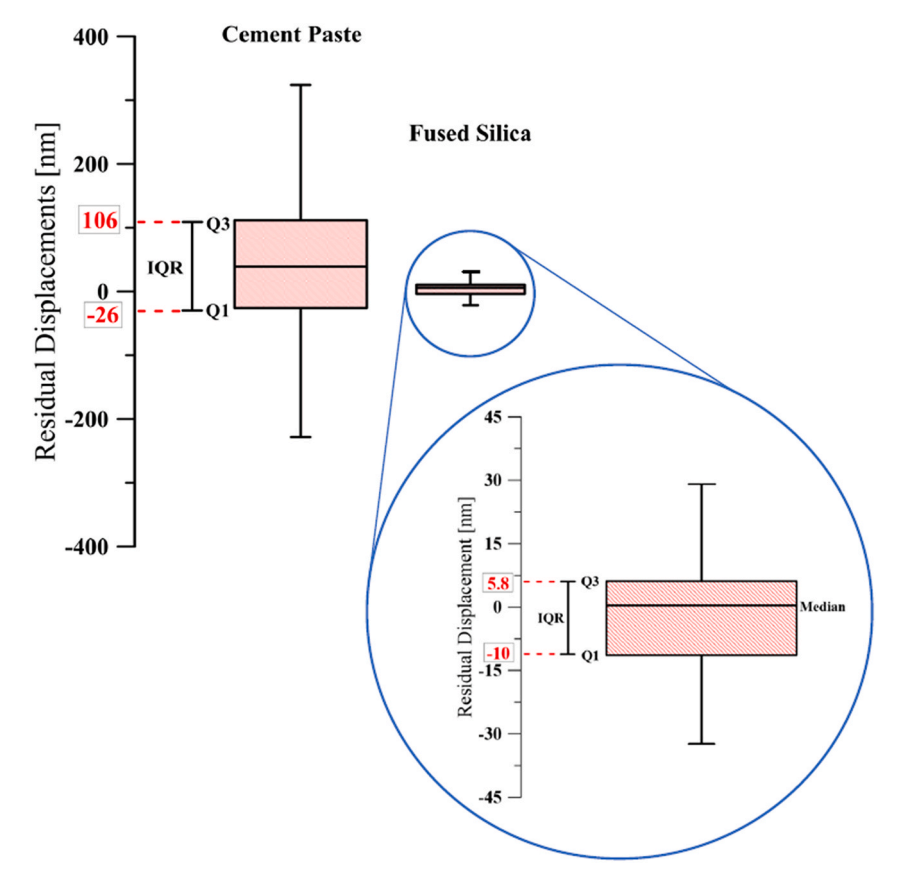


Fig. 10. Whisker box plot comparing the residual errors between the experimentally acquired data and the optimum model obtained via the inverse minimization problem for the neat cement paste and fused silica.

primarily originating from the indentation portion of the total displacement $\triangle_{\rm I}$. However, such events have random nature, and their effect on the parameters estimates in the inverse analysis is reduced by (a) taking multiple measurements along the beam length (see Fig. 8b), and (b) proper selection of the indentation probe size and force such that the characteristic size of the indentation interaction volume and the contact area is significantly larger than the characteristic size of the statistically dominant heterogeneities (Fig. 1a). If a significant violation of the latter is encounter e.g. shallow indents with a small contact radius, the measured response will reflect the local variations of the indentation response attributable to microstructural phases rather than bulk material. As a consequence, the applicability of the proposed model, which assumes statistically homogeneous properties along the micro-beam may be severely compromised.

5. Summary and conclusions

The presented work was focused on the development and evaluation of micro-bending method of materials characterization at micro and mesoscale. Analytical developments were accompanied by the experimental work which validated the proposed method and demonstrated its potential to test elastic and flexural strength properties of cement-based composites using a standard micro-indentation tester. The main outcomes of this study can be summarized as follows:

- 1. The proposed analytical model, which is formulated within the framework of the beam on an elastic foundation (Winkler type), accurately describes the functional relationship between applied force, beam deflection, and physical and geometrical characteristics of the beam material and the support. The accuracy of the proposed methods was demonstrated through the extensive analysis of reference materials spanning from ceramics to metals.
- 2. The inverse problem minimization was used in the indirect estimation of elastic modulus of tested material, support stiffness, as well as displacement component due to indentation. The estimates of elastic modulus show high reliability and accuracy, giving micro-bending estimates within a 5% error relative to the macroscopic estimates obtained in standard ASTM testing.
- 3. Despite a significantly increased level of microstructure heterogeneity, normal weight and lightweight cement pastes were successfully tested with the micro-bending approach for elastic and flexural properties. The stability of the inverse minimization problem was not affected by the measurement errors originating from material

- heterogeneity and surface roughness, thus, resulting in stable values of elastic modulus which show excellent agreement with those experimentally obtained via standard uniaxial compression testing of large scale specimens.
- 4. The proposed micro-bending approach is easily adaptable to the standard microindenter tester allowing for taking advantage of the available high-resolution force and displacement sensors. Thus, making this technique a complementary characterization tool to instrumented indentation testing of cementitious matrices and systems alike.

Although the presented work discusses the method application to static loading, it can be comprehended that given the advancement in the available indentation testing instruments other load-case scenarios can be easily realized. Therefore, one could pursue the investigation of other phenomena and related properties, e.g., fracture toughness, creep, or fatigue, just to name a few.

Credit author statement

Santiago El Awad: Investigation, Formal analysis, Validation, Methodology, Writing – original draft, Writing – review & editing, Damian Stefaniuk: Investigation, Methodology, Software, Formal analysis, Writing – review & editing, Konrad J. Krakowiak: Conceptualization, Writing – review & editing, Funding acquisition, Formal analysis, Methodology, Project administration, Resources, Supervision.

Declaration of competing interest

The authors declare that they have no known competing financial interests or personal relationships that could have appeared to influence the work reported in this paper.

Acknowledgement

The research team is grateful for the financial support of the lead author by Anton Paar USA, Inc., through Anton Paar Scholarship for Undergraduate Students. Also, the support of the Dwight David Eisenhower Transportation Fellowship Program (DDETFP) for Mr. El Awad is acknowledged. This work was also supported by the National Science Foundation under Grants No. 1825921. DS was supported by the Foundation for Polish Science (FNP).

APPENDIX I. DERIVATION OF THE MODEL EQUATIONS

We assume here, the portion of the cantilever beam that rests on the elastic foundation is modeled using a series of non-interacting linear-elastic springs distributed along the support length, Winkler type Fig. A1.1. The collective behavior of springs is expressed using foundation stiffness parameter k.

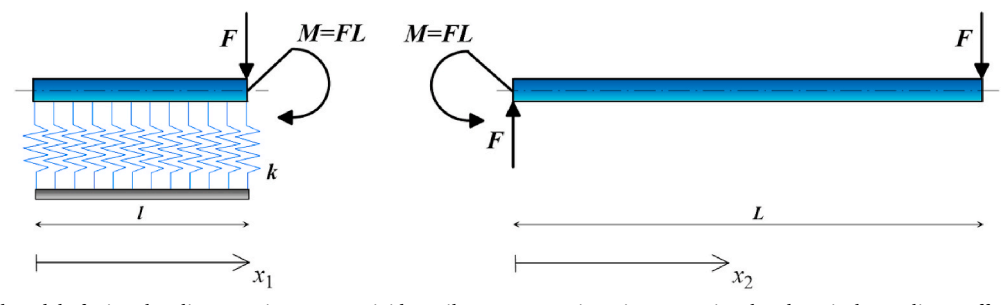


Fig. A1.1. Mechanical model of micro-bending experiment. Non-rigid cantilever support gives rise to rotational and vertical compliance effects which are accounted for by assuming beam resting on the elastic foundation which is modeled using series of non-interacting linear-elastic springs distributed along the support length, Winkler type (Hetényi, 1971).

Considering the equilibrium of an infinitely small segment of the beam, the fourth-degree differential equation Eq. (A1.1) describes the beam

deflection in the domain $x_1 \in 0, l$, and its general solution reads Eq. (A1.2).

$$EI\frac{\partial^4 w_1(x_1)}{\partial x_1^4} + kw_1(x_1) = 0$$
 Eq. A1.1

$$w_1(x_1) = e^{\lambda x_1} (A\cos(\lambda x_1) + B\sin(\lambda x_1)) + e^{-\lambda x_1} (C\cos(\lambda x_1) + D\sin(\lambda x_1))$$
 Eq. A1.2

The constant λ quantifies the flexural rigidity of the beam Eq. (A1.3), where E is the Young's modulus of the beam material, I is the area moment of inertia.

$$\lambda = \sqrt[4]{\frac{k}{4FI}}$$
 Eq. A1.3

Four constants, A through D are determined from the boundary conditions, Eq. A1.4a-d.

$$EIw_{\parallel\parallel_{\mathrm{I}}=0}^{\prime\prime}=0$$
 Eq. A1.4a

$$Elw_{\parallel |_{\Sigma} = l}^{"} = -F$$
 Eq. A1.4b

$$EIw''_{1|x_1=l} = \text{F-L}$$
 Eq. A1.4c

$$EIw_{1|x_1=0}^{m}=0$$
 Eq. A1.4d

Ultimately, for the given micro-bending problem at hand, one is primarily interested in the beam deflection, w_1 and rotation, θ_1 , at $x_1 = l$. These are explicitly given in the following forms (Hetényi, 1971):

$$w_{1,F} = \frac{2F}{k} \lambda \left(\frac{\sinh(\lambda l) \cosh(\lambda l) - \sin(\lambda l) \cos(\lambda l)}{\sinh^2(\lambda l) - \sin^2(\lambda l)} \right)$$
 Eq. A1.5a

$$w_{1,M} = \frac{2F}{k}L\lambda^2 \left(\frac{\sinh^2(\lambda l) + \sin^2(\lambda l)}{\sinh^2(\lambda l) - \sin^2(\lambda l)}\right)$$
 Eq. A1.5b

$$\theta_{1,F} = -\frac{2F}{k}\lambda^2 \left(\frac{\sinh^2(\lambda l) + \sin^2(\lambda l)}{\sinh^2(\lambda l) - \sin^2(\lambda l)} \right)$$
 Eq. A1.5c

$$\theta_{1,M} = -\frac{4F}{k}L\lambda^3 \left(\frac{\sinh(\lambda l)\cosh(\lambda l) + \sin(\lambda l)\cos(\lambda l)}{\sinh^2(\lambda l) - \sin^2(\lambda l)} \right)$$
 Eq. A1.5d

where $w_{1,F}$ and $w_{1,M}$ is the deflection due to the concentrated force and moment, respectively. Likewise, $\theta_{1,F}$ and $\theta_{1,M}$ are the corresponding cross-section rotations. Hence, the total vertical displacement, and the rotation angle at the support end where the beam enters the cantilever domain x_2 read:

$$w_{1|x_1=l} = w_{1,F} + w_{1,M}$$
,

$$\theta_{1|x_1=l} = \theta_{1,F} + \theta_{1,M}$$
 . Eq. A1.6b

Derived edge displacement and rotation are used to calculate the cantilever deflection at the point of load application at the distance L from the elastic support, see Fig. A1.1. To obtain its analytical expression, we consider the beam deflection equation, Eq. (A1.7), which w_2 must satisfy in the domain of x_2 :

$$EIw_2'' = -M_a$$
,

where the distribution of bending moment is the linear function of x_2 :

$$M_a = -F(L - x_2)$$
.

Combining Eq. (A1.7) and Eq. (A1.8) we obtain the curvature-moment relationship of the cantilever beam, which upon integration results in the general solution with two integration constants, Eq. (A1.9):

$$EIw_2 = -\frac{1}{6}Fx_2^3 + \frac{1}{2}FLx_2^2 + Ax_2 + B$$
,

where constants A and B are calculated taking into account displacement and rotation continuity conditions:

$$w_{1|x_1=l} = w_{2|x_2=0}$$
 Eq. A1.10a

$$heta_{1|x_1=l} = heta_{2|x_2=0}$$
 Eq. A1.10b

where given relationships Eq. A1.11 both constants read as:

$$A = EI(\theta_{1,F} + \theta_{1,M}),$$
 Eq. A1.11a

$$B = EI(w_{1,F} + w_{1,M}).$$
 Eq. A1.11b

Finally, the cantilever deflection at the point of the load application, $x_2 = L$, is expressed as:

$$\Delta = \underbrace{\frac{\mathrm{FL}^3}{3\mathrm{EI}}}_{\Delta_{-p}} + \underbrace{L(\theta_{1,F} + \theta_{1,M})}_{\Delta_{\phi}} + \underbrace{(w_{1,F} + w_{1,M})}_{\Delta_{V}}$$
 Eq. A.1.12

where Δ_B is the deflection solely due to cantilever bending, Δ_{θ} and Δ_{V} are deflection components originating from the rotational and translational compliance of the elastic support.

APPENDIX II. DEFLECTION AT THE ELASTIC SUPPORT

An auxiliary problem of the beam on the elastic foundation with the concentrated load at mid-span is addressed here, Fig. A2.1. Its solution, we are looking for the beam deflection at the point of load application, is used to reduce overall uncertainty on micro-bending model parameters estimated in the inverse-problem analysis. It is noted, from the experimental perspective an investigator can perform an indentation in the center of the elastic support with ease and at no time cost, and such measurements provide additional benefit in constraining the solution of the inverse problem.

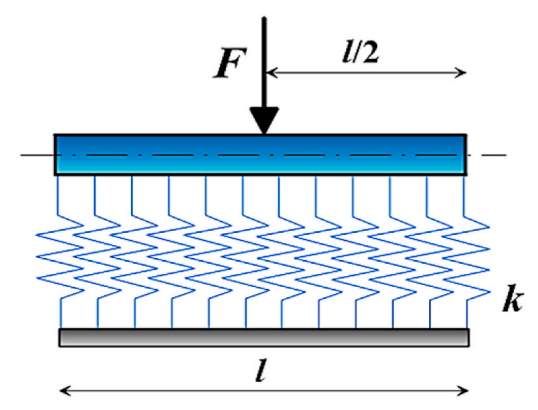


Fig. A2.1. Mechanical model of finite-length, Winkler type beam subject to center point load.

Similarly, to the previous case presented in Appendix I, the displacement in the mid-span is expressed in the general form fourth-order differential equation, Eq. (A1.1). However, in this case, the unknown constants are found considering the new set of boundary conditions:

$$EIw_{1|x_{1}=0}^{"}=0$$
 Eq. A2.1a

$$EIw_{1|x_{1}=l}^{\prime\prime}=0$$
 Eq. A2.1b

$$Elw_{1|0}^{"}=0$$
 Eq. A2.1c

$$EIw_{1|x_{1}=1}^{m}=0$$
 Eq. A2.1d

As a result, the analytical solution for the deflection caused by the force acting in the middle of the elastic foundation is given by Eq. (A2.2), (Hetényi, 1971).

$$\Delta = \frac{F\lambda}{2k} \left(\frac{\cosh(\lambda l) + \cos(\lambda l) + 2}{\sinh(\lambda l) - \sin(\lambda l)} \right).$$
 Eq. A2.2

References

- Asif, S.A.S., Pethica, J.B., 1998. Nano-scale viscoelastic properties of polymer materials. In: Cammarata, R.C., Nastasi, M.A., Busso, E.P., Oliver, W.C. (Eds.), Thin-Films-Stresses and Mechanical Properties VII, vol. 505. Materials Research Society, Pittsburgh, PA, pp. 103–108. https://doi.org/10.1557/PROC-505-103.
- ASM, 1990. Properties and Selection: Nonferrous Alloys and Special-Purpose Materials, ASM Handbook, vol. 2. ASM International, The Materials Information Company. https://doi.org/10.31399/asm.hb.v02.9781627081627.
- ASTM International, 2016. C293/C293M-16 Standard Test Method for Flexural Strength of Concrete (Using Simple Beam with Center-Point Loading). ASTM International, West Conshohocken, PA. https://doi.org/10.1520/C0293 C0293M-16.
- ASTM International, 2018. C78/C78M-18 Standard Test Method for Flexural Strength of Concrete (Using Simple Beam with Third-Point Loading). ASTM International, West Conshohocken, PA. https://doi.org/10.1520/C0078_C0078M-18.
- Bazant, Z.P., Novak, D., 2001. Proposal for standard test of modulus of rupture of concrete with its size dependence. ACI Mater. J. 98 (1), 79–87.
- Callister Jr., W.D., 2007. Materials Science and Engineering, an Introduction, seventh ed. John Wiley & Sons, Inc.

- Chavent, G., 2010. Nonlinear Least Squares for Inverse Problems: Theoretical Foundations and Step-by-step Guide for Applications. Springer Science & Business Media. https://doi.org/10.1007/978-90-481-2785-6.
- Cook, R.F., Phaar, G.M., 1990. Direct observation and analysis of indentation cracking in glassess and cermics. J. Am. Ceram. Soc. 73 (4), 787–817. https://doi.org/10.1111/ j.1151-2916.1990.tb05119.x.
- Constantinides, G., Ulm, F.J., 2004. The effect of two types of C-S-H on the elasticity of cement-based materials: results from nanoindentation and micromechanical modeling. Cement Concr. Res. 34, 67–80. https://doi.org/10.1016/S0008-8846(03) 00230-8.
- Constantinides, G., Ravi Chandran, K.S., Ulm, F.J., Van Vliet, K.J., 2006. Grid indentation analysis of composite microstructure and mechanics: principles and validation. Mater. Sci. Eng. 430, 189–202. https://doi.org/10.1016/j. msea.2006.05.125.
- Doerner, M.F., Nix, W.D., 1986. A method for interpreting the data from depth sensing indentation instruments. J. Mater. Res. 1, 4. https://doi.org/10.1557/ JMR.1986.0601.
- Engineering Edge, 2020. Engineers Edge, LLC, Modulus of Elasticity Young's Modulus Strength for Metals Iron and Steel. https://www.engineersedge.com/manufacturing_spec/properties_of_metals_strength.htm. (Accessed 28 October 2020).

- EuroInox, 2007. Stainless Steel: Tables and Technical Properties, Materials and Applications Series, vol. 5. EuroInox, The European Stainless Steel Development Association, 2007.
- Fischer-Cripps, A.C., 2004. Contact mechanics. In: Nanoindentation. Mechanical Engineering Series. Springer, New York, NY. https://doi.org/10.1007/978-1-4757-5943-3 1.
- Gan, Y., Zhang, H., Šavija, B., Schlangen, E., van Breugel, K., 2018. Static and fatigue tests on cementitious cantilever beams using nanoindenter. Micromachines 9, 630. https://doi:10.3390/mi9120630.
- Gan, Y., Vandamme, M., Zhang, H., Chen, Y., Schlangen, E., van Breugel, K., Śavija, B., 2020. Micro-cantilever testing on the short-term creep behavior of cement paste at micro-scale. Cement Concr. Res. 134, 106105. https://doi.org/10.1016/j. cemconres.2020.106105.
- He, L.H., Swain, M.V., 2007. Nanoindentation derived stress-strain properties of dental materials. Dent. Mater. J. 23, 814. https://doi.org/10.1016/j.dental.2006.06.017.
- Hetényi, M., 1971. Beams on Elastic Foundation: Theory with Applications in the Fields of Civil and Mechanical Engineering. University of Michigan.
- Johnson, K.L., 1985. Contact Mechanics. Cambridge University Press. https://doi.org/ 10.1017/CB09781139171731.
- Krakowiak, K.J., Nannapaneni, R.G., Moshiri, A., Phatak, T., Stefaniuk, D., Sadowski, L., Abdolhosseini Qomi, M.J., 2020. Engineering of high strength and low thermal conductivity cementitious composites with hollow glass microspheres for hightemperature high-pressure applications. Cem.Con.Comp. 108, 103514. https://doi. org/10.1016/j.cemconcomp.2020.103514.
- Lucas, B.N., Oliver, W.C., 1999. Indentation power-law creep of high-purity indium. Metall. Mater. Trans. 30, 601. https://doi.org/10.1007/s11661-999-0051-7.
- Miller, M., Bobko, C., Vandamme, M., Ulm, F.J., 2008. Surface roughness criteria for cement paste nanoindentation. Cement Concr. Res. 38, 467–476. https://doi.org/ 10.1016/j.cemconres.2007.11.014.
- Mindes, S., Young, J.F., Darein, D., 2002. Concrete, second ed. Prentice Hall.
- Němeček, J., Králík, V., Šmilauer, V., Polívka, L., Jäger, A., 2016. Tensile strength of hydrated cement paste phases assessed by micro-bending tests and nanoindentation.

- Cement Concr. Compos. 73, 164–173. https://doi.org/10.1016/j.cemconcomp.2016.07.010.
- Novak, D., Bazant, Z.P., Vitek, J.L., 2002. In: Bilek, V., Kersner, Z. (Eds.), Experimental-analytical Size-dependent Prediction of Modulus of Rupture of Concrete. Non-traditional Cement and Concrete, pp. 387–393.
- Oliver, W.C., Pharr, G.M., 1992. An improved technique for determining hardness and elastic modulus using load and displacement sensing indentation experiments. J. Mater. Res. 7, 6. https://doi.org/10.1557/JMR.1992.1564.
- Oyen, M.L., Cook, R.F., 2003. Load-displacement behavior during sharp indentation of viscous-elastic-plastic materials. J. Mater. Res. 18 (1), 139–150. https://doi.org/ 10.1557/PROC-649-01.5.
- Oyen, M.L., 2006. Nanoindentation hardness of mineralized tissues. J. Biomech. 39, 2699. https://doi.org/10.1016/j.jbiomech.2005.09.011.
- Oyen, M.L., Cook, R.F., 2009. A practical guide for analysis of nanoindentation data. J. Mech. Behav. Biomed. 2, 396. https://doi.org/10.1016/j.jmbbm.2008.10.002.
- Sneddon, J.N., 1965. The relation between load and penetration in the axisymmetric boussinesq problem for a punch of arbitrary profile. Int. J. Eng. Sci. 3, 47. https://doi.org/10.1016/0020-7225(65)90019-4.
- Tabor, D., 1951. The Hardness of Metals. Oxford University Press, London. https://doi. org/10.1038/170818b0
- Timoshenko, S.P., Goodier, J.N., 1970. Theory of Elasticity, third ed. McGraw-Hill Kogakusha, Tokyo, pp. 398–422. https://doi.org/10.1016/C2009-0-25521-8.
- VanLandingham, M.R., 2003. Review of instrumented indentation. J. Res. Natl. Inst. Stand. Technol. 108, 249. https://doi.org/10.6028/jres.108.024.
- Walley, S.M., 2012. Historical origins of indentation hardness testing. Mater. Sci. Technol. 28, 1028. https://doi.org/10.1179/1743284711Y.0000000127.
- Zaoui, A., 2002. Continuum micromechanics: survey, 8-8-816 J. Eng. Mech. 128 (8). https://doi.org/10.1061/(ASCE)0733-9399(2002)128:8(808).
- Zok, F.W., 2006. Development in oxide fiber composites. J. Am. Ceram. Soc. 89 (11), 3309–3324. https://doi.org/10.1111/j.1551-2916.2006.01342.x.